

Structural behavior, crystal chemistry, and phase transitions in substituted leucite: High-resolution neutron powder diffraction studies

DAVID C. PALMER,^{1,*} MARTIN T. DOVE,¹ RICHARD M. IBBERSON,² AND BRIAN M. POWELL³

¹Department of Earth Sciences, University of Cambridge, Downing Street, Cambridge, CB2 3EQ, U.K.

²ISIS Facility, Rutherford-Appleton Laboratory, Chilton, Didcot, Oxfordshire, OX11 0QX, U.K.

³AECL Research, Chalk River Laboratories, Chalk River, Ontario, K0J 1J0, Canada

ABSTRACT

High-resolution neutron powder diffraction was used to study phase transitions in the leucite phases of KAlSi_2O_6 , $\text{RbAlSi}_2\text{O}_6$, $\text{CsAlSi}_2\text{O}_6$, and KFeSi_2O_6 . The temperature-dependent structural behavior involves two mechanisms: relaxation of the tetrahedral framework about channel cations, and slowly changing T-O bond lengths. The high-temperature cubic phase is characterized by a fully-extended tetrahedral framework; thermal expansion occurs by an increase in mean T-O bond lengths. On decreasing temperature, a displacive phase transition to tetragonal symmetry is manifested by an optic instability; twisting of tetragonal prisms of corner-linked $(\text{Al,Si})\text{O}_4$ tetrahedra about $[001]$ leads to collapse of the $\langle 111 \rangle$ structural channels and concomitant volume reduction.

INTRODUCTION

Leucite, KAlSi_2O_6 , has been the subject of a remarkable proliferation of research papers in recent years (Boysen 1990; Brown et al. 1987; Dove et al. 1993a; Hatch et al. 1990; Heaney and Veblen 1990; Lange et al. 1986; Murdoch et al. 1988; Palmer 1990a, 1990b; Palmer et al. 1988, 1989, 1990; Palmer and Salje 1990; Phillips et al. 1989; Phillips and Kirkpatrick 1994). Though not a major rock-forming mineral, leucite is nevertheless interesting to geologists because of its petrogenesis and occurrence in regions of alkaline volcanism and continental rifting. The mineral is interesting in its own right because of its complex phase-transition behavior, manifested in the fine-scale twinning that has for so long been a diagnostic feature. Leucite structures are extremely tolerant toward ionic substitutions (Bayer 1973; Taylor and Henderson 1968; Galli et al. 1978), and it is the considerable structural flexibility with respect to changing composition, temperature, and pressure that makes leucite particularly important from a crystal-chemical viewpoint.

The leucite structure comprises a framework of corner-sharing $(\text{Al,Si})\text{O}_4$ tetrahedra, arranged in fourfold, sixfold, and eightfold rings. The sixfold rings are arranged axially, forming structural channels parallel to $\langle 111 \rangle$. Such a channel arrangement is typical of feldspathoids (Merlino 1984) and some zeolites. In comparison with feldspars and other framework structures without channels, feldspathoids show many possibilities for structural modification, including framework distortion, channel collapse, and ionic mobility.

Naturally occurring leucite crystallizes in the cubic

phase, with space group $Ia3d$ (Peacor 1968). On cooling below $T_c \approx 938$ K, there is a phase transition to a tetragonal form, which has space group $I4_1/a$ at room temperature (Mazzi et al. 1976). There are indications, however, that an additional tetragonal phase is stable over a narrow temperature interval. The first evidence for this was the discovery of two DTA peaks near the supposed inversion temperature (Faust 1963). This observation was later verified by DSC scans in several leucite samples (Lange et al. 1986) and attributed to the two phase transitions $Ia3d \rightarrow I4_1/acd$ and $I4_1/acd \rightarrow I4_1/a$.

X-ray diffraction studies showed that the two phase transitions are displacive in character and lead to large spontaneous strains (Palmer et al. 1989). These produce the distinctive lamellar twins that are generally visible on an optical scale. A second type of twinning, induced by the tetragonal-tetragonal inversion, is only observed on the electron-microscopic scale (Palmer et al. 1988; Palmer 1990a; Heaney and Veblen 1990). The distortion of the unit cell may be rationalized in terms of ferroelastic (i.e., shape-changing) and isotropic (volume-changing) parts. The anomalous (and continuous) volume decrease at low temperatures is a result of the $I4_1/acd \rightarrow I4_1/a$ phase transition.

There had been suggestions that Al-Si ordering plays a role in the phase transition (Brown et al. 1987; Murdoch et al. 1988; Phillips et al. 1989), but modeling studies (Dove et al. 1993a) have shown that Al-Si ordering is not required for the transitions to occur. Furthermore, lattice strains occur in the absence of any long-range order, and any ordering produces strains that are considerably smaller than the actual spontaneous strain observed.

Dielectric studies (Palmer and Salje 1990) have shown that the phase transitions are associated with critical be-

* Present address: Department of Earth Sciences, The Open University, Walton Hall, Milton Keynes, MK7 6AA, U.K.

TABLE 1. Characterization of leucite compounds used in this work

| Leucite specimen | Composition | Unit cell at 298 K | | |
|-----------------------------------|--|--------------------|--------------|----------------------------|
| | | <i>a</i> (Å) | <i>c</i> (Å) | <i>V</i> (Å ³) |
| Natural | K _{0.97} Al _{1.01} Fe _{0.01} Si _{1.99} O ₆ | 13.0548(2) | 13.7518(2) | 2343.69(1) |
| Rb-substituted | Rb _{0.99} Cs _{0.01} Al _{0.99} Si _{1.99} O ₆ | 13.2918(2) | 13.7412(2) | 2427.69(1) |
| Cs-substituted | Cs _{0.98} K _{0.01} Ca _{0.01} Al _{1.00} Si _{1.98} O ₆ | 13.6524(4) | 13.7216(4) | 2557.54(1) |
| KFeSi ₂ O ₆ | K _{0.90} Fe _{0.95} Si _{2.01} O ₆ | 13.2036(2) | 13.9545(3) | 2432.76(1) |

Note: Natural leucite is from Rome, Italy. See text for preparation of other samples.

havior of the K channel cations. Boysen (1990) envisaged a progressive delocalization of the channel cations as the phase-transition temperature is approached. It was suggested that the intermediate tetragonal phase is stabilized by delocalization of the K cations. Palmer and Salje (1990) proposed that the progressive “melting” of the K⁺ substructure, combined with a framework distortion, was responsible for the $I4_1/a \rightarrow I4_1/acd$ phase transition. An acoustic shear distortion was proposed for the change $I4_1/acd \rightarrow Ia3d$ (Palmer 1990b).

Several questions still remain unanswered. What is the structural behavior at the unit-cell level? What distortion patterns, at the microscopic level, are reflected in the macroscopic order parameter? Can various aspects of the transition behavior, e.g., the volume anomaly or the thermodynamic character, be modified by changing composition? To address these questions, we studied the structural aspects of the phase transitions over a wide range of temperature for different chemical compositions: natural leucite (KAlSi₂O₆), synthetic KFeSi₂O₆, and ion-exchanged RbAlSi₂O₆ and CsAlSi₂O₆.

To collect structural data, we used high-resolution neutron powder diffraction, mostly with a high-intensity, pulsed neutron spallation source. High-resolution neutron powder diffraction offers several advantages in comparison with more conventional single-crystal X-ray techniques: short data-collection times, simple experimental geometries (allowing heating and cooling), and no problems resulting from sample twinning.

EXPERIMENTAL PROCEDURES

Sample preparation

Natural leucite was collected from the Roman Volcanic Province, Italy, by one of the authors (D.C.P.) and Ciriaco Giampaolo (Università di Roma). The locality was a road cutting at Quarto Miglio, near Rome, where a gravel deposit contained abundant leucite phenocrysts. Large quantities of crystals were collected and cleaned using an ultrasonic bath. Any crystals with traces of weathering or containing inclusions were rejected. The chemical composition was determined using electron microprobe analysis at the University of Cambridge. Many different crystals were analyzed, but no appreciable differences could be detected, neither was there any evidence of chemical zoning or alteration. The mean composition is given in Table 1.

The same natural leucite also served as starting mate-

rial for the preparation of Rb- and Cs-substituted leucite samples. It was decided to prepare these materials using ion exchange, following unsuccessful attempts at hydrothermal synthesis (using the method of Hamilton and Henderson 1968) and dry synthesis (using oxide mixtures), which resulted in run products that were never fully stoichiometric, being somewhat deficient in the alkali cation. Although X-ray analysis seemed to imply well-crystallized products, these samples proved unsatisfactory for neutron diffraction because of broadening of high-angle diffraction peaks.

To produce the ion-exchanged leucite samples, we took a silica-glass tube, welded one end shut, and added finely powdered natural leucite. A large excess (thirty times the mole fraction of leucite) of either RbBr or CsBr was then added. The bromides were purchased from Aldrich Chemicals: The RbBr was claimed to be 99% pure and the CsBr 99.9% pure. The tube was then evacuated and sealed. The resulting capsule was annealed in a vertical tube furnace at 1073 K for 3 d, during which time the bromide melted and ion exchange occurred. On removal from the furnace, the leucite crystals were separated from the bromide by dissolving the latter in distilled water. Electron microprobe analysis of these samples was conducted at the Natural History Museum, London, under the guidance of Frances Wall. The crystals were found to be homogeneous throughout, and there were no significant differences between separate grains (see Table 1 for compositions of the crystals).

Although we could not synthesize satisfactory samples of Rb- and Cs-substituted leucite, we did manage to produce KFeSi₂O₆ leucite using dry synthesis. High-purity ferric oxide, silica, and potassium carbonate were mixed and ground together in a ball mill for 30 min, until a fine, even powder remained. This mixture was melted in a zirconia crucible at 1473 K. (The use of platinum at this stage was scrupulously avoided because of the risk of Fe adsorption, which would alter the stoichiometry of the final glass.) Our glass was a deep red color, and was fully crystallized following annealing at 1073 K for 8 d in an Fe-soaked platinum crucible. The crystals were characterized by X-ray and neutron diffraction and found to show sharp diffraction peaks, even at high order; diffraction patterns were virtually identical to those obtained from natural leucite. Transmission electron microscopy revealed extensive lamellar twinning, strikingly similar to that observed in natural leucite. Most of the crystals were

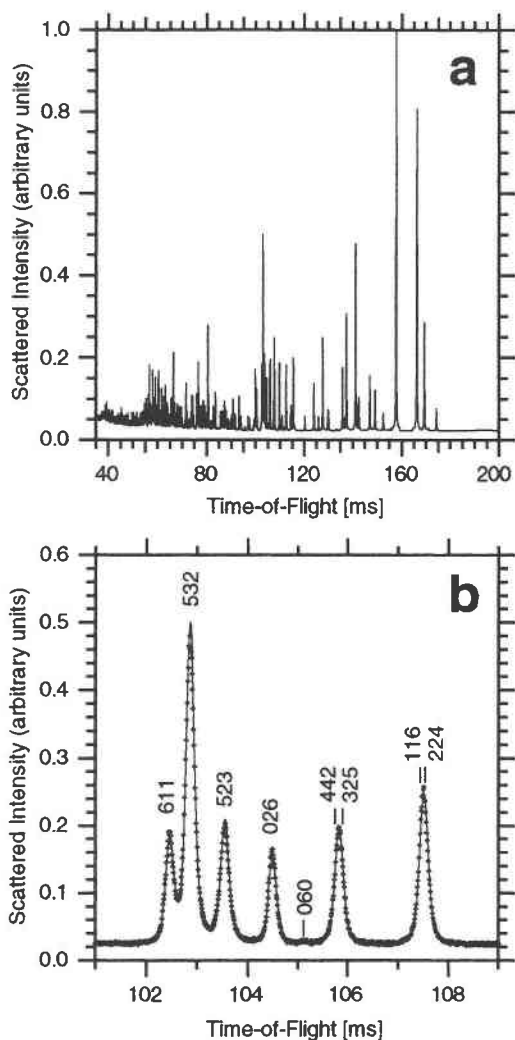


FIGURE 1. Time-of-flight neutron diffraction patterns for natural leucite at 298 K. (a) Complete spectrum used for structure refinement. There is a linear relation between time-of-flight and interplanar d value; the limits correspond to 0.83–3.73 Å. (b) Expanded region of the spectrum from 2.09–2.26 Å. The observed data are shown as plus signs, and the Bragg peaks are indexed; the solid curve is the fitted spectrum, derived from Rietveld refinement.

<200 μm in diameter, although larger crystals formed at the top of the crucible. The crystals were predominantly yellow to red in color, suggesting that the Fe was present as Fe^{3+} rather than Fe^{2+} . This was borne out by electron microprobe analysis (Table 1). The material has a 10% K deficiency, presumably caused by alkali loss during the annealing process.

Minute quantities of another phase were detected optically as thin red flakes within some of the leucite grains. Electron microprobe analysis of the flakes revealed them to be Fe_2O_3 . These could not be detected by X-ray powder diffraction, but neutron diffraction spectra showed two weak peaks not corresponding to any leucite reflections

and presumably caused by the second phase. These peaks were omitted from structure refinements.

Neutron diffraction

Structural data on natural, synthetic, and ion-exchanged leucite samples were obtained using two instruments. All high-temperature measurements, and the 4 K leucite experiment, were performed on the High Resolution Powder Diffractometer (HRPD) at the ISIS spallation neutron source at the Rutherford-Appleton Laboratory (U.K.). ISIS is a pulsed source, and HRPD exploits this property by measuring the flight time of neutrons scattering from the sample through a large fixed angle. The long flight path (98 m) enables a high resolution ($\Delta d/d \approx 4 \times 10^{-4}$) to be obtained. Data were collected for reflections with d values between 0.7–2.4 Å; lower order reflections could not be measured with the configuration used in the experiment. The raw data were normalized for the energy distribution of the neutrons in a single pulse, dividing the spectra by the spectrum recorded by a monitor positioned in the incoming beam. A typical normalized diffraction pattern is illustrated in Figure 1a.

The experiments on Cs-substituted leucite used a cryostat and were performed on the 30-element array diffractometer on the E13 beam hole at Chalk River Laboratory (Ontario, Canada). This is a standard angle-dispersive diffractometer. Data were collected for scattering angles up to 120° with neutron wavelength of 1.4994 Å.

Data analysis

Structure refinements were performed using a program developed at ISIS that can handle both time-of-flight and angle-dispersive data. The refinement of the time-of-flight data used a peak-shape function that included an appropriate instrumental function convoluted with Gaussian or Lorentzian profiles representative of sample-broadening effects. It was found that, because the resolution of the data was sufficiently high, the Lorentzian contributions to the peak shape were important. Standard Gaussian profiles were used for the angle-dispersive data. At all temperatures there was a significant diffuse background scattering, which was modeled using Chebychev polynomials. Anisotropic atomic displacement factors were included in the refinements, using the formalism $\exp[-\frac{1}{4}(h^2a^{*2}B_{11} + k^2b^{*2}B_{22} + l^2c^{*2}B_{33} + 2hka^*b^*B_{12} + 2hka^*c^*B_{13} + 2klb^*c^*B_{23})]$. The full refinements of the low-temperature tetragonal structures included 30 atomic coordinates and 60 anisotropic displacement factors, plus a scale factor, unit-cell parameters, four peak-shape functions, and up to ten background parameters. We also sometimes included two site-occupancy factors for the tetrahedral sites (the third occupancy factor was constrained by the values for the other two sites).

With refinements as large as these from powder data, it is essential that the starting model be as close to the end result as possible. Because of the narrow peak width of HRPD we needed to determine accurate cell param-

ters for each temperature before beginning the refinement. We used the structure model of Mazzi et al. (1976) in our first refinement of the room-temperature structure of leucite. We then used the results as the starting structure for the next highest temperature and continued this procedure systematically with increasing temperature. On approaching the transition temperature the structures changed more rapidly between runs. Moreover, closer to the transition temperature the distortions of the structure from the ideal cubic structure became smaller and the effects on the diffraction patterns were also less significant. We therefore needed to "nurse" the refinements of the higher temperature data by first refining only the coordinates that varied the most with temperature and allowing all the coordinates to vary only at a later stage in the refinements.

With the exception of the room-temperature, Cs-substituted leucite refinement (a very small tetragonal distortion), we did not use isotropic displacement factors because the refinements were generally much poorer than those obtained with the anisotropic displacement factors. The diagonal coefficients were varied after convergence of the atomic coordinates, and the off-diagonal coefficients were included in the final stages of the refinements. We found in some cases near the transition temperature that the displacement factors could not be varied at the same time as the atomic coordinates; the refinement could not converge properly in these cases, although it was clear that the parameter set was never far from the least-squares minimum. Instead we found that an iterative procedure, in which we alternately varied the coordinates and displacement factors, always gave satisfactory convergence. For the substituted leucite we used initial trial structures obtained from natural leucite at a temperature with spontaneous strain similar to that at room temperature in the substituted leucite. A representative fitted diffraction pattern is shown in Figure 1b.

ROOM-TEMPERATURE CRYSTAL STRUCTURES

Natural leucite

The crystal structure of natural leucite, L999, refined at room temperature, is shown in Figure 2, with structural data listed in Table 2. There are no significant differences between this structure and the tetragonal structure reported by Mazzi et al. (1976).

Our study offered the opportunity of providing independent structural information on the degree of Al-Si tetrahedral site ordering: Neutron diffraction is better suited to the determination of Al-Si site occupancies than X-ray diffraction because the neutron-scattering lengths for these two atoms are very different. However, for neutron powder diffraction, there is the difficulty of extracting meaningful site occupancies from the profile refinement. We found strong correlations between the site occupancies and the displacement parameters, and we were unable to refine site occupancies for the room-temperature data.

In an attempt to overcome the correlation problem, we

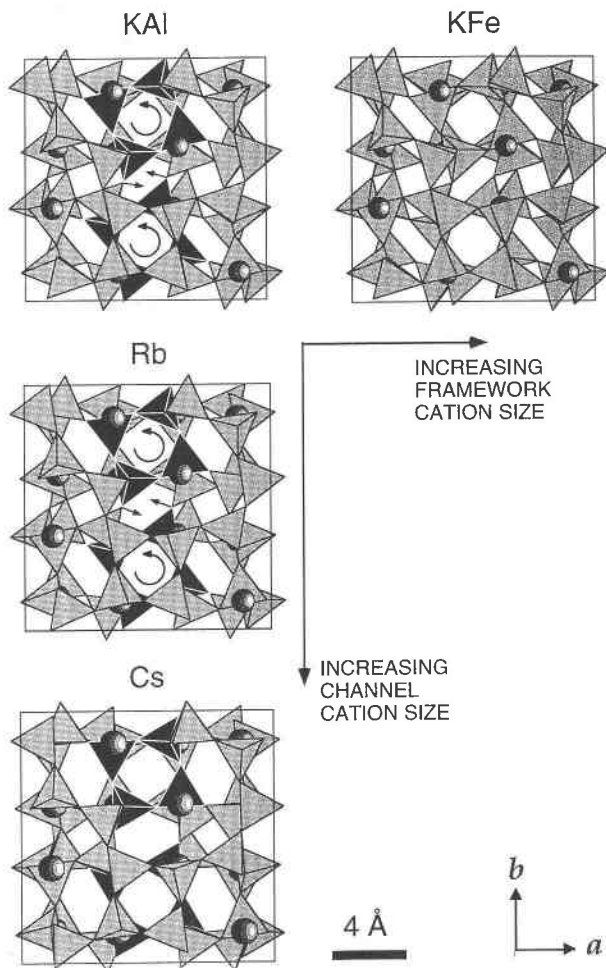


FIGURE 2. Crystal structures of different leucite compounds at 298 K. Tetrahedra represent $(\text{Al,Si})\text{O}_4$ and $(\text{Fe,Si})\text{O}_4$ groups; shaded spheres represent channel cations (K,Rb,Cs). Decreasing the size of the channel cations from Cs to K results in a twisting of the tetrahedral framework around $[001]$, with rotations of the fourfold rings (indicated in black) and crumpling of the $\langle 111 \rangle$ structural channels. By contrast, changing the size of the framework cations (e.g., by replacing Al with Fe) has virtually no effect on the framework distortion, although the overall cell volume does increase.

performed extended data collection at 4 K (run number 3277). The structural data are given in Table 3.¹ Even at this low temperature, it was not possible to refine meaningful site occupancies. It must be stressed that this is not a failure of the refinement process per se: There is the intractable problem that beyond relatively low scattering angles the diffracted intensity is very low, which effec-

¹ A copy of Tables 3 and 10–40 may be ordered as Document AM-97-633 from the Business Office, Mineralogical Society of America, 1015 Eighteenth Street NW, Suite 601, Washington, DC 20036. Please remit \$5.00 in advance for the microfiche. Movies of the phase transitions, in QuickTime format, for the Macintosh computer, are available on request from the first author.

TABLE 2. Positional coordinates, anisotropic displacement parameters, and typical refinement errors for natural leucite at 298 K (expt. no. 3003)

| Site | <i>x</i> | <i>y</i> | <i>z</i> | <i>B</i> ₁₁ | <i>B</i> ₂₂ | <i>B</i> ₃₃ | <i>B</i> ₂₃ | <i>B</i> ₁₃ | <i>B</i> ₁₂ |
|------|-------------|-------------|-------------|------------------------|------------------------|------------------------|------------------------|------------------------|------------------------|
| K | 0.3659 | 0.3637 | 0.1169 | 2.98 | 2.02 | 7.98 | -0.57 | 0.03 | -0.50 |
| T1 | 0.0574 | 0.3969 | 0.1665 | 0.58 | 0.07 | 0.71 | -0.09 | 0.44 | -0.05 |
| T2 | 0.1675 | 0.6116 | 0.1287 | 0.24 | 0.84 | 0.08 | 0.42 | -0.22 | -0.15 |
| T3 | 0.3930 | 0.6420 | 0.0862 | 0.16 | 0.60 | 0.69 | -0.76 | -0.14 | -0.18 |
| O1 | 0.1324 | 0.3141 | 0.1099 | 2.53 | 1.27 | 3.19 | -0.59 | 0.35 | 0.59 |
| O2 | 0.0908 | 0.5112 | 0.1308 | 2.18 | 1.80 | 1.61 | 0.07 | -0.06 | -0.50 |
| O3 | 0.1461 | 0.6808 | 0.2278 | 1.85 | 1.28 | 0.93 | -0.13 | 0.48 | -0.14 |
| O4 | 0.1331 | 0.6851 | 0.0348 | 1.47 | 2.26 | 1.27 | 0.56 | -0.04 | 0.23 |
| O5 | 0.2889 | 0.5756 | 0.1204 | 0.68 | 1.14 | 2.27 | -0.04 | 0.38 | 0.03 |
| O6 | 0.4836 | 0.6172 | 0.1673 | 0.81 | 1.34 | 1.02 | 0.27 | -0.19 | -0.05 |
| Site | $\sigma(x)$ | $\sigma(y)$ | $\sigma(z)$ | $\sigma(B_{11})$ | $\sigma(B_{22})$ | $\sigma(B_{33})$ | $\sigma(B_{23})$ | $\sigma(B_{13})$ | $\sigma(B_{12})$ |
| K | 0.0009 | 0.0007 | 0.0010 | 0.4030 | 0.4622 | 0.7166 | 0.4944 | 0.4628 | 0.4015 |
| T1 | 0.0006 | 0.0006 | 0.0005 | 0.4349 | 0.3180 | 0.3380 | 0.3244 | 0.3392 | 0.3505 |
| T2 | 0.0006 | 0.0005 | 0.0006 | 0.3935 | 0.3903 | 0.3827 | 0.3301 | 0.3160 | 0.3297 |
| T3 | 0.0006 | 0.0006 | 0.0006 | 0.3422 | 0.3753 | 0.4743 | 0.3164 | 0.3040 | 0.2630 |
| O1 | 0.0005 | 0.0004 | 0.0004 | 0.3406 | 0.2621 | 0.3790 | 0.3040 | 0.2581 | 0.2270 |
| O2 | 0.0004 | 0.0004 | 0.0005 | 0.3060 | 0.3165 | 0.3862 | 0.2934 | 0.2357 | 0.1842 |
| O3 | 0.0003 | 0.0004 | 0.0004 | 0.2305 | 0.2645 | 0.2414 | 0.2349 | 0.2074 | 0.2143 |
| O4 | 0.0005 | 0.0004 | 0.0004 | 0.3387 | 0.3085 | 0.2766 | 0.2330 | 0.2434 | 0.2536 |
| O5 | 0.0004 | 0.0004 | 0.0005 | 0.2798 | 0.2660 | 0.3016 | 0.2243 | 0.2376 | 0.2122 |
| O6 | 0.0004 | 0.0005 | 0.0004 | 0.2355 | 0.2742 | 0.2925 | 0.2720 | 0.2014 | 0.2193 |

Note: Space group: $I4_1/a$; cell parameters: $a = 13.05476$, $c = 13.75182$ Å; $\chi^2 = 1.8996$; $\sigma_{\max}(xyz) = 0.0003$; $\sigma_{\max}(B_{ij}) = 0.17$.

tively masks the effects of any ordering. We therefore assumed disordered Al-Si distributions for all subsequent refinements, including those of the ion-exchanged samples.

Rb- and Cs-substituted leucite

The structure of Rb-substituted leucite was satisfactorily refined using the $I4_1/a$ positional parameters of natural leucite as starting values (Table 4).

Our Cs-substituted leucite results (Table 5) provide the first reported occurrence of a tetragonal structure at room temperature, rather than the cubic structure claimed by all previous investigators (Taylor and Henderson 1968; Hirao and Soga 1982; Kosorukov and Nadal 1986). At room temperature, the tetragonal distortion in our Cs-substituted leucite is small in comparison with similar distortions in natural and Rb-substituted leucite samples. Closely-overlapping diffraction peaks made structure refinement nontrivial, and we were forced to use isotropic displacement factors to ensure that the refinement converged.

The room-temperature structures of the leucite samples

in the ion-exchange series K-Rb-Cs are shown in Figures 2 and 3, and bond-length and angle data are given in Tables 6 and 7. The unit-cell dimensions are highly sensitive to the size of the channel (W site) cation (Fig. 4; Table 8). Individual (Al,Si)O₄ tetrahedra are far less sensitive: Substituting Cs⁺ for K⁺ causes an 11% change in the mean W-O bond length (a measure of the effective channel diameter) but a mere 0.6% change in the mean T-O bond length (T denotes the tetrahedral cation Al,Si or Fe). The tetrahedra may therefore be regarded as essentially rigid, so that the structural response to increasing size of W is a relaxation of the framework around the W site.

We now examine the framework relaxation in more detail. Figure 2 contains projections of the leucite structures at 298 K, emphasizing the tetragonal prisms parallel to *c*. These prisms consist of square-planar rings of four tetrahedra (two pointing up, and two pointing down) at either end, which are connected by two additional tetrahedra. As the W cation decreases in size, the tetragonal prisms (parallel to *c*) respond by twisting about their axes.

TABLE 4. Positional coordinates and anisotropic displacement parameters for Rb-substituted leucite at 298 K (expt. no. 2830)

| Site | <i>x</i> | <i>y</i> | <i>z</i> | <i>B</i> ₁₁ | <i>B</i> ₂₂ | <i>B</i> ₃₃ | <i>B</i> ₂₃ | <i>B</i> ₁₃ | <i>B</i> ₁₂ |
|------|----------|----------|----------|------------------------|------------------------|------------------------|------------------------|------------------------|------------------------|
| K | 0.3654 | 0.3636 | 0.1221 | 3.45 | 2.64 | 4.93 | -0.31 | -0.27 | -0.22 |
| T1 | 0.0643 | 0.3926 | 0.1656 | 3.13 | 2.11 | 3.67 | -0.54 | 0.54 | 0.47 |
| T2 | 0.1684 | 0.6060 | 0.1283 | 3.35 | 1.95 | 3.23 | 0.20 | 0.08 | -0.88 |
| T3 | 0.3911 | 0.6447 | 0.0864 | 2.65 | 1.78 | 1.81 | 0.05 | 0.45 | -0.22 |
| O1 | 0.1324 | 0.3054 | 0.1099 | 2.64 | 2.67 | 1.88 | 0.30 | -0.05 | 0.53 |
| O2 | 0.1039 | 0.5015 | 0.1265 | 1.78 | 2.02 | 3.06 | 0.21 | 0.38 | 0.05 |
| O3 | 0.1398 | 0.6729 | 0.2260 | 1.63 | 2.47 | 2.12 | 0.49 | -0.18 | 0.02 |
| O4 | 0.1317 | 0.6761 | 0.0338 | 1.17 | 0.93 | 1.97 | -0.26 | 0.01 | -0.39 |
| O5 | 0.2899 | 0.5808 | 0.1237 | 0.41 | 0.51 | 0.81 | 0.24 | 0.40 | -0.20 |
| O6 | 0.4822 | 0.6174 | 0.1638 | 0.66 | 0.76 | 0.62 | -0.74 | 0.01 | 0.09 |

Note: Space group: $I4_1/a$; cell parameters: $a = 13.29180$, $c = 13.74118$ Å; $\chi^2 = 1.9211$; $\sigma_{\max}(xyz) = 0.0002$; $\sigma_{\max}(B_{ij}) = 0.14$.

TABLE 5. Positional coordinates and isotropic displacement parameters for Cs-substituted leucite at 298 K (expt. no. 2828)

| Site | <i>x</i> | <i>y</i> | <i>z</i> | <i>B</i> _{iso} |
|------|----------|----------|----------|-------------------------|
| Cs | 0.3701 | 0.3698 | 0.1238 | 2.63 |
| T1 | 0.0801 | 0.3832 | 0.1625 | 0.72 |
| T2 | 0.1667 | 0.5958 | 0.1234 | 0.43 |
| T3 | 0.3852 | 0.6555 | 0.8050 | 1.29 |
| O1 | 0.1347 | 0.2883 | 0.1084 | 2.02 |
| O2 | 0.1289 | 0.4814 | 0.1160 | 2.39 |
| O3 | 0.1183 | 0.6502 | 0.2204 | 2.24 |
| O4 | 0.1274 | 0.6577 | 0.0300 | 2.57 |
| O5 | 0.2874 | 0.5923 | 0.1293 | 2.32 |
| O6 | 0.4764 | 0.6160 | 0.1540 | 2.51 |

Note: Space group: *I*₄/*a*; cell parameters: *a* = 13.65199, *c* = 13.72126 Å; χ^2 = 3.8347; $\sigma_{\max}(xyz)$ = 0.0007; $\sigma_{\max}(B_{\text{iso}})$ = 0.17.

The lower fourfold tetrahedral ring rotates relative to the overlying ring (illustrated in Fig. 2 for K and Rb- and Cs-substituted leucite samples, where the tetrahedral rings at the bases of the prism elements are shaded and their relative rotations indicated by arrows). The effect of the twisting is an elongation of the prisms parallel to the rotation axis [001], accompanied by contraction of the prism perpendicular to this axis. In addition to this contraction, individual prisms rotate about [001]. Rotations of adjacent prisms are in the opposite sense, so the net result is a significant decrease in the cell dimensions perpendicular to [001], i.e., *a* and *b* are reduced. The concomitant elongation of the structural prisms parallel to [001] explains the slight increase in the *c* dimension with decreasing size of the channel cation.

The twisting motions of the tetrahedral rings are consistent with the symmetry *T*_{1g} (in the intermediate phase of leucite, this becomes *A*_{2g}, which has the representation *R*₃, i.e., a twist parallel to *c*). The importance of this twisting distortion to the overall structural behavior is illustrated in Figure 4: Increasing the channel-cation size has very little effect on the *c* parameter but drastically changes the *a* parameter. The twisting of tetragonal prisms and the resultant change in the unit-cell dimensions is thus a case of rotational-translation coupling.

KFeSi₂O₆

Synthetic KFeSi₂O₆ was first described by Faust (1936) and was later studied by Hirao et al. (1976), Lange et al. (1986), Palmer (1990b), and Bell and Henderson (1994). We refined the structure of KFeSi₂O₆ using the *I*₄/*a* leucite positional parameters as starting values (Table 9). During the course of the structure refinement we tried to determine Fe-Si site occupancies. As was the case for natural leucite, we found that freeing the site occupancies prevented the refinement from converging, and we were forced to fix the occupancies. We therefore used disordered Fe-Si distributions for all refinements of KFeSi₂O₆.

In comparison with natural leucite, KFeSi₂O₆ has a larger unit cell (Fig. 2). The mean T-O distances are greater, with virtually no change in the mean W-O dis-

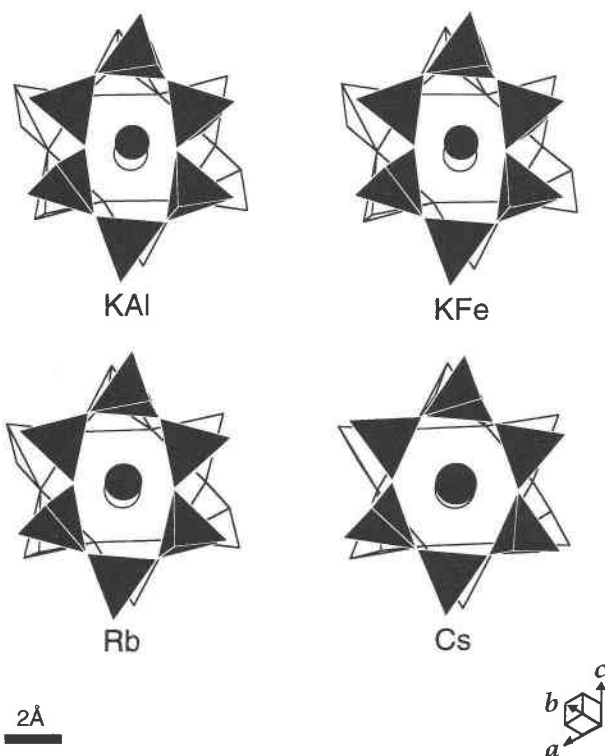


FIGURE 3. Channel structures of different leucite compounds at 298 K. Decreasing the size of the channel cation from Cs to K distorts the structural channels (reducing the mean W-O bond distance), with an associated off-centering of the channel cations parallel to $[\bar{1}12]$. The crystal structure for KFeSi₂O₆ is virtually identical to that of natural leucite (i.e., replacing Al³⁺ with Fe³⁺ leaves the channel structure essentially undisturbed).

tances (Table 6). The expansion in the unit-cell volume of KFeSi₂O₆ is therefore directly attributed to an increase in the size of the tetrahedral sites. This is to be expected given the larger size of Fe³⁺ (ionic radius 0.49 Å for tetrahedral coordination, according to Shannon 1976) in comparison with Al³⁺ (ionic radius 0.39 Å).

The substitution of Fe for Al in the leucite framework causes a slight distortion of the tetrahedra, as revealed by the O-T-O bond angles (Table 7), with the most distorted site being T3. This site is the largest of the three sites and is arguably the site most likely to contain Fe (though we found no evidence for this preference). The T-O-T bond angles are reduced from a mean value of 137.8° in natural leucite to 135.7° in KFeSi₂O₆ (Table 7), as the larger, Fe-bearing tetrahedral framework collapses around the K channel sites.

TEMPERATURE-DEPENDENT STRUCTURAL BEHAVIOR

Unit-cell parameters

All the leucite samples show a progressive convergence of the tetragonal *a* and *c* cell parameters on increasing temperature, leading to a reversible, displacive

TABLE 6. Bond-length data (Å) for the tetrahedral (T) and channel (W) cations in natural and substituted leucite samples at 298 K

| Bond | Natural leucite | Rb-substituted leucite | Cs-substituted leucite | KFeSi ₂ O ₆ leucite |
|-------------|-----------------|------------------------|------------------------|---|
| T1-O1(T1)* | 1.654(9) | 1.657 | 1.668 | 1.650 |
| T1-O1'(T1') | 1.638(10) | 1.635 | 1.642 | 1.680 |
| T1-O2(T2) | 1.631(9) | 1.632 | 1.628 | 1.651 |
| T1-O4(T2) | 1.639(9) | 1.636 | 1.623 | 1.694 |
| Mean T1-O | 1.641(9) | 1.640 | 1.637 | 1.668 |
| T2-O2(T1) | 1.649(9) | 1.632 | 1.647 | 1.697 |
| T2-O3(T3) | 1.657(9) | 1.655 | 1.662 | 1.710 |
| T2-O4(T1') | 1.670(10) | 1.671 | 1.626 | 1.658 |
| T2-O5(T3') | 1.657(9) | 1.650 | 1.651 | 1.691 |
| Mean T2-O | 1.658(9) | 1.652 | 1.644 | 1.689 |
| T3-O3(T2) | 1.647(10) | 1.640 | 1.619 | 1.682 |
| T3-O5(T2') | 1.679(10) | 1.672 | 1.701 | 1.726 |
| T3-O6(T3) | 1.657(10) | 1.666 | 1.655 | 1.713 |
| T3-O6'(T1') | 1.660(10) | 1.653 | 1.641 | 1.667 |
| Mean T3-O | 1.661(10) | 1.658 | 1.651 | 1.697 |
| W-O1** | 3.116(13) | 3.196 | 3.407 | 3.152 |
| W-O1' | | | 3.460 | |
| W-O2 | 2.999(11) | 3.263 | | 2.948 |
| W-O3 | 2.987(13) | 3.139 | 3.392 | 3.006 |
| W-O4 | 2.940(14) | 3.068 | 3.310 | 2.985 |
| W-O5 | 2.944(11) | 3.057 | 3.242 | 2.956 |
| W-O6 | 3.025(14) | 3.133 | 3.289 | 3.026 |
| Mean W-O | 3.002(13) | 3.143 | 3.350 | 3.012 |

Note: The natural leucite data include errors in the bond lengths (calculated from the errors in fractional coordinates and the unit-cell dimensions), as indicators of the typical uncertainty.

* The second tetrahedral site bonded to the O atom is given in parentheses.

** The six shortest bonds are given; note that for Cs-substituted leucite, with very small tetragonal distortion, the pattern of closest O atoms is slightly different in comparison with that of the other leucite samples studied.

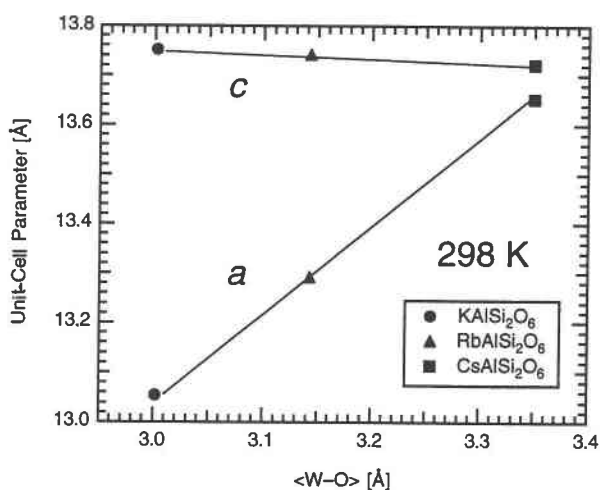


FIGURE 4. Effect of the distortion caused by tetragonal prism twisting on the unit-cell parameters of substituted leucite. Decreasing the size of the W cation (indicated here by its effective size in the channel site, measured from the mean W-O bond distances) causes a very large decrease in *a*, with a smaller increase in *c*.

TABLE 7. Bond angles (°) for the tetrahedral (T) sites at 298 K

| Bond angle | Natural leucite | Rb-substituted leucite | Cs-substituted leucite | KFeSi ₂ O ₆ leucite |
|-------------|-----------------|------------------------|------------------------|---|
| O1-T1-O1' | 113.3 | 112.0 | 111.9 | 112.8 |
| O1-T1-O2 | 107.3 | 107.0 | 106.4 | 109.4 |
| O1-T1-O4 | 111.1 | 110.8 | 111.0 | 110.9 |
| O1'-T1-O2 | 107.3 | 108.5 | 108.9 | 105.8 |
| O1'-T1-O4 | 105.4 | 106.4 | 106.0 | 104.4 |
| O2-T1-O4 | 112.5 | 112.3 | 112.8 | 113.5 |
| Mean O-T1-O | 109.5 | 109.5 | 109.5 | 109.5 |
| O2-T2-O3 | 108.4 | 110.4 | 110.4 | 106.0 |
| O2-T2-O4 | 107.9 | 108.0 | 109.9 | 106.7 |
| O2-T2-O5 | 110.9 | 109.9 | 106.8 | 111.3 |
| O3-T2-O4 | 106.1 | 105.2 | 105.5 | 105.1 |
| O3-T2-O5 | 111.8 | 111.4 | 111.7 | 110.0 |
| O4-T2-O5 | 111.5 | 111.6 | 112.5 | 116.9 |
| Mean O-T2-O | 109.4 | 109.4 | 109.5 | 109.3 |
| O3-T3-O5 | 109.9 | 110.5 | 110.2 | 111.3 |
| O3-T3-O6 | 109.7 | 110.2 | 113.3 | 108.0 |
| O3-T3-O6' | 109.3 | 108.8 | 107.8 | 110.7 |
| O5-T3-O6 | 106.7 | 106.3 | 102.8 | 102.5 |
| O5-T3-O6' | 110.4 | 110.3 | 109.9 | 111.3 |
| O6-T3-O6' | 110.8 | 110.7 | 112.8 | 109.7 |
| Mean O-T3-O | 109.5 | 109.5 | 109.5 | 108.9 |
| T1-O1-T1' | 143.6 | 145.5 | 146.7 | 143.2 |
| T1-O2-T2 | 153.5 | 156.8 | 152.2 | 151.5 |
| T2-O3-T3 | 129.2 | 132.5 | 143.3 | 126.9 |
| T1-O4-T2 | 140.6 | 142.1 | 145.1 | 137.7 |
| T2-O5-T3 | 130.3 | 134.1 | 138.7 | 125.2 |
| T3-O6-T3' | 129.8 | 132.7 | 137.8 | 129.7 |
| Mean T-O-T | 137.8 | 140.6 | 144.0 | 135.7 |

phase transition to a high-temperature cubic structure. Replacing K with larger channel cations causes an increase in the unit-cell volume, a decrease in the tetragonal *c-a* splitting, and a lower cubic-to-tetragonal phase-transition temperature (Fig. 5; Table 8). This is similar to the effect of increasing temperature. On the other hand, substitution of larger framework cations (replacing Al³⁺ with Fe³⁺) causes almost isotropic expansion; the *a* and *c* dimensions increase, and the *c-a* splitting remains virtually unchanged.

The phase transitions may be described in group theoretical terms. For the two phase transitions $Ia3d \rightarrow I4_1/acd$ and $I4_1/acd \rightarrow I4_1/a$, the active representations are E_g and A_{2g} , respectively. The E_g representation is the symmetry of a ferroelastic distortion (with strain components $\epsilon_1 - \epsilon_2$ and $2\epsilon_3 - \epsilon_1 - \epsilon_2$), whereas A_{2g} corresponds to an optic distortion. This distortion involves a nonsymmetry-breaking volume strain (A_{1g} representation), which couples to the square of the corresponding order parameter ($A_{2g} \otimes A_{2g} = A_{1g}$).

One might also consider a direct transition: $Ia3d \rightarrow I4_1/a$. The active representation is T_{1g} , which also corresponds to an optic instability. This produces both ferroelastic (E_g -type) and volume distortions (A_{1g} -type), which couple to the square of the associated order parameter. The effects of a single cubic-to-tetragonal phase transition would therefore be qualitatively similar to those of a stepwise transition, with the absence of an intermediate phase.

A convenient way of quantifying the macroscopic transition behavior is to measure the temperature dependence of the spontaneous strain. Using the same strain analysis

TABLE 8. Unit-cell parameters (Å) for natural and substituted leucite samples

| <i>T</i> (K) | Natural leucite | | Rb-substituted leucite | | Cs-substituted leucite | | KFeSi ₂ O ₆ leucite | |
|--------------|-----------------|------------|------------------------|------------|------------------------|------------|---|------------|
| | <i>a</i> | <i>c</i> | <i>a</i> | <i>c</i> | <i>a</i> | <i>c</i> | <i>a</i> | <i>c</i> |
| 4 | 12.9952(6) | 13.7645(6) | | | | | | |
| 20 | | | | | 13.5265(3) | 13.7594(3) | | |
| 80 | | | | | 13.5397(3) | 13.7518(3) | | |
| 150 | | | | | 13.5640(3) | 13.7413(3) | | |
| 298 | 13.0548(2) | 13.7518(2) | 13.2918(2) | 13.7412(2) | 13.6524(4) | 13.7216(4) | 13.2036(2) | 13.9545(3) |
| 323 | | | | | 13.6701(3) | 13.7158(4) | 13.2128(4) | 13.9524(5) |
| 333 | | | | | 13.6729(3) | 13.7129(4) | | |
| 343 | | | | | 13.6795(3) | 13.7098(4) | | |
| 353 | | | | | 13.6861(3) | 13.7066(5) | | |
| 363 | | | | | 13.693(1) | 13.701(1) | | |
| 368 | | | | | 13.697(1) | 13.701(1) | | |
| 373 | 13.0897(9) | 13.7530(9) | 13.3238(5) | 13.7310(5) | 13.6993(3) | 13.6993(3) | 13.2345(3) | 13.9457(3) |
| 378 | | | | | 13.7008(5) | 13.7008(5) | | |
| 383 | | | | | 13.7015(5) | 13.7015(5) | | |
| 393 | | | | | 13.7019(4) | 13.7019(4) | | |
| 423 | | | 13.3495(1) | 13.7230(3) | 13.7022(5) | 13.7022(5) | | |
| 473 | 13.116(1) | 13.739(1) | 13.3772(6) | 13.7160(6) | 13.7062(6) | 13.7062(6) | 13.2739(3) | 13.9333(3) |
| 523 | | | 13.4051(2) | 13.7057(6) | | | 13.2926(6) | 13.9279(7) |
| 553 | | | 13.4273(4) | 13.6966(4) | | | | |
| 563 | | | 13.4340(6) | 13.6927(6) | | | | |
| 573 | 13.158(1) | 13.731(1) | 13.4398(6) | 13.6907(6) | 13.7093(5) | 13.7093(5) | 13.3192(3) | 13.9165(3) |
| 623 | | | 13.4761(2) | 13.6739(3) | | | 13.3457(6) | 13.9065(7) |
| 663 | | | 13.5134(4) | 13.6561(5) | | | | |
| 673 | 13.205(1) | 13.721(1) | 13.5277(8) | 13.6488(8) | | | 13.3781(3) | 13.8927(4) |
| 683 | | | 13.5366(2) | 13.6440(3) | | | | |
| 693 | | | 13.5464(2) | 13.6388(3) | | | | |
| 703 | | | 13.5570(2) | 13.6324(3) | | | | |
| 713 | | | 13.5677(2) | 13.6261(1) | | | | |
| 723 | | | 13.5694(1) | 13.6197(2) | | | 13.4111(7) | 13.8737(8) |
| 728 | | | 13.5791(2) | 13.6192(3) | | | | |
| 733 | | | 13.5837(3) | 13.6165(3) | | | | |
| 738 | | | 13.5903(3) | 13.6122(3) | | | | |
| 743 | | | 13.5957(2) | 13.6091(4) | | | | |
| 748 | | | | | | | 13.4375(8) | 13.8589(9) |
| 753 | | | 13.6033(2) | 13.6033(2) | | | | |
| 763 | | | 13.6057(2) | 13.6057(2) | | | | |
| 773 | 13.271(1) | 13.702(1) | | | | | 13.4672(8) | 13.8589(9) |
| 783 | | | | | | | 13.478(1) | 13.829(1) |
| 793 | | | | | | | 13.490(1) | 13.816(1) |
| 803 | | | 13.6114(2) | 13.6114(2) | | | 13.505(1) | 13.807(1) |
| 813 | | | 13.6115(1) | 13.6115(1) | | | 13.524(1) | 13.794(1) |
| 823 | 13.313(1) | 13.683(1) | | | | | 13.541(1) | 13.781(1) |
| 833 | | | | | | | 13.564(1) | 13.762(1) |
| 843 | | | | | | | 13.587(1) | 13.743(1) |
| 853 | | | 13.6152(2) | 13.6152(2) | | | 13.663(1) | 13.663(1) |
| 863 | | | | | | | 13.6642(3) | 13.6642(3) |
| 873 | 13.368(2) | 13.646(2) | | | | | 13.6661(3) | 13.6661(3) |
| 883 | 13.401(2) | 13.636(2) | | | | | 13.6725(3) | 13.6725(3) |
| 893 | 13.430(3) | 13.610(4) | | | | | | |
| 903 | | | 13.6192(2) | 13.6192(2) | | | | |
| 923 | 13.517(3) | 13.537(4) | | | | | 13.6806(2) | 13.6806(2) |
| 943 | 13.535(1) | 13.535(1) | | | | | 13.6837(2) | 13.6837(2) |
| 948 | | | | | | | | |
| 953 | | | 13.6218(1) | 13.6218(1) | | | | |
| 963 | 13.539(1) | 13.539(1) | | | | | | |
| 973 | 13.542(1) | 13.542(1) | | | | | 13.6882(4) | 13.6882(4) |
| 983 | 13.542(1) | 13.542(1) | | | | | | |
| 993 | 13.543(1) | 13.543(1) | | | | | | |
| 1003 | 13.546(1) | 13.546(1) | | | | | | |
| 1013 | 13.545(1) | 13.545(1) | | | | | | |
| 1023 | 13.550(1) | 13.550(1) | | | | | | |
| 1050 | | | | | | | 13.6965(8) | 13.6965(8) |

as Palmer et al. (1989), we rationalized the behavior of the total spontaneous strain, ϵ_{tot} , in terms of a symmetry-breaking ferroelastic strain, ϵ_e , and a nonsymmetry-breaking volume strain, ϵ_a . The total spontaneous strain is defined from the extrapolation of the cubic cell parameter, a_0 , into the tetragonal stability phase:

$$\epsilon_{\text{tot}} = \sqrt{\left(\frac{c - a_0}{a_0}\right)^2 + 2\left(\frac{a - a_0}{a_0}\right)^2}$$

$$\epsilon_a = \sqrt{3} \frac{a_0 - (c + 2a)/3}{a_0}$$

$$\epsilon_e = \epsilon_{\text{tot}} - \epsilon_a$$

TABLE 9. Positional coordinates and anisotropic displacement parameters for KFeSi_2O_6 leucite at 298 K (expt. no. 3757)

| Site | x | y | z | B_{11} | B_{22} | B_{33} | B_{23} | B_{13} | B_{12} |
|------|--------|--------|--------|----------|----------|----------|----------|----------|----------|
| K | 0.3650 | 0.3624 | 0.1162 | 8.47 | 2.05 | 10.68 | -3.25 | -4.34 | 0.07 |
| T1 | 0.0579 | 0.3964 | 0.1665 | 0.36 | 1.59 | 3.13 | -0.90 | -0.44 | 0.00 |
| T2 | 0.1673 | 0.6123 | 0.1265 | 1.39 | 2.77 | 0.27 | 0.10 | -0.70 | -0.58 |
| T3 | 0.3905 | 0.6444 | 0.0843 | 1.88 | 1.99 | 0.61 | -0.45 | 0.14 | -0.55 |
| O1 | 0.1310 | 0.3155 | 0.1087 | 7.06 | 3.29 | 8.41 | 0.22 | 1.46 | -1.07 |
| O2 | 0.0862 | 0.5128 | 0.1329 | 3.18 | 6.20 | 5.35 | 0.04 | -1.20 | -0.56 |
| O3 | 0.1463 | 0.6828 | 0.2274 | 4.18 | 3.22 | 3.91 | 0.56 | 2.12 | 1.03 |
| O4 | 0.1282 | 0.6843 | 0.0364 | 2.91 | 6.04 | 2.48 | 0.86 | 1.04 | 0.52 |
| O5 | 0.2892 | 0.5729 | 0.1234 | 3.92 | 2.45 | 4.42 | -1.54 | 0.78 | -0.58 |
| O6 | 0.4813 | 0.6183 | 0.1684 | 1.79 | 3.49 | 4.80 | -0.51 | -0.58 | 1.57 |

Note: Space group: $I4_1/a$; cell parameters: $a = 13.20357$, $c = 13.95446$ Å; $\chi^2 = 1.1668$; $\sigma_{\max}(xyz) = 0.0020$; $\sigma_{\max}(B_{ij}) = 1.44$.

For a single phase transition, $Ia3d \rightarrow I4_1/a$, we would expect symmetry-breaking and nonsymmetry-breaking strains. The ferroelastic strain is proportional to the macroscopic order parameter for this zone-center phase transition.

Rb-substituted leucite. Rb-substituted leucite shows a continuous phase transition on increasing temperature.

Figure 6 demonstrates a quadratic dependence of the strain components with temperature. This transition may therefore be classified, in Landau terminology, as being tricritical in character, with critical exponent $\beta = 1/4$. The two strain components show virtually identical temperature behavior (Fig. 6), which is expected if there is a single phase transition. Contrast this behavior with that

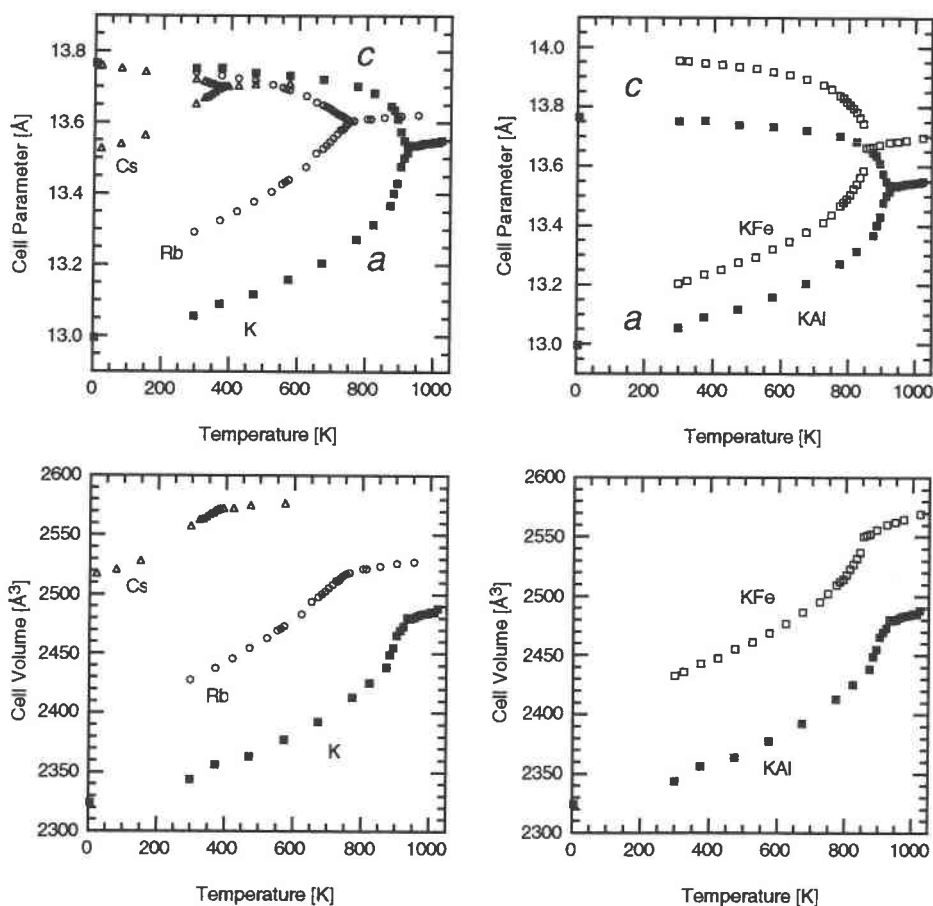


FIGURE 5. Effects of temperature and composition on the unit-cell parameters of leucite. (**top left**) The effect of larger channel cations (Rb and Cs). (**bottom left**) Unit-cell volumes for natural leucite and Rb- and Cs-substituted leucite. (**top right**) The effect of larger framework cations. Synthetic leucite, in which all the Al^{3+} is replaced with Fe^{3+} , is compared with natural leucite. (**bottom right**) Unit-cell volumes for natural leucite and KFeSi_2O_6 leucite. The error bars for all measurements are smaller than the sizes of the data points.

for pure leucite (Palmer et al. 1989), in which the volume strain extrapolates to zero at a temperature lower than that at which the ferroelastic strain extrapolates to zero, consistent with the existence of an intermediate $I4_1acd$ tetragonal phase.

Cs-substituted leucite. Despite the very small spontaneous strain in Cs-substituted leucite, the temperature evolution of the cell parameters is similar to that for Rb-substituted leucite, and the spontaneous strain indicates a tricritical phase transition (Fig. 6).

KFeSi₂O₆ leucite. The distortion of the tetrahedral framework may be modified by changing the sizes of the tetrahedral cations. The behaviors of the cell parameters (Fig. 5) is superficially similar to those for natural leucite. However, a pronounced hysteresis on heating and cooling and a discontinuity in the cell parameters (and volume) indicate that KFeSi₂O₆ shows a first-order phase transition. This is consistent with earlier DSC work (Lange et al. 1986), which revealed a sharp peak at T_c , with a 16 K hysteresis. During our present work, a hysteresis was detected following heating and cooling of the sample; the cell parameters presented here were obtained during heating of the sample.

In comparison with natural leucite, KFeSi₂O₆ has larger tetrahedral sites, causing the framework to crumple around the K ions. This crumpling distortion explains why, at 298 K, the ferroelastic strain in KFeSi₂O₆ (plotted in Fig. 6) is significantly greater than that for natural leucite (Palmer et al. 1989) and more than double the volume strain.

Structural data

Tables 3 and 10 present the temperature-dependent structural data for all the samples studied.

Effects of temperature: leucite. In the leucite structure, fourfold tetrahedral rings are linked to form prisms, parallel to the a , b , and c axes. These rings remain rigid at all temperatures, but at low temperatures their coupled rotations distort the sixfold tetrahedral rings (decreasing the T-O-T bond angles), visualized as a crumpling of the $\langle 111 \rangle$ structural channels (Fig. 7).

The progressive crumpling of the channel structure can be quantified by measuring the effective channel-cation (W site) size (given by the mean W-O distance) with increasing temperature (Fig. 8). At 298 K, the mean K-O distance in leucite, 3.00 Å, is similar to that for feldspars (2.93–3.00 Å). However, there is a large expansion (~10%) in channel size with increasing temperature in the tetragonal phase, until the channels become fully inflated as the structure attains cubic symmetry.

The channel distortion is accompanied by slight movements of the K ions (Fig. 7). At low temperatures, collapse of the structural channels forces a puckering of the K-ion distribution, so that the ions are offset parallel to $[112]$. On increasing temperature, the off-centering vectors gradually rotate about the channel axis. In the intermediate $I4_1acd$ phase, the off-centering is parallel to $[110]$, which is perpendicular to the 4 K arrangement, and

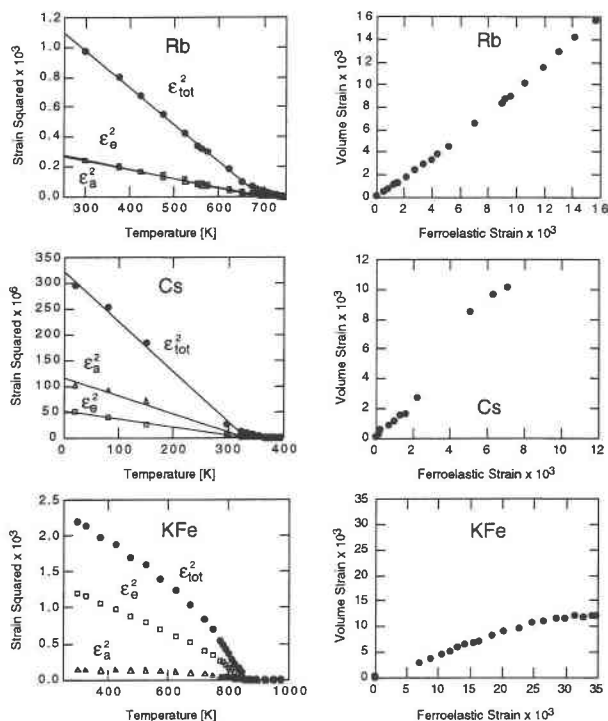


FIGURE 6. Graphs on the left show the effects of temperature and composition on the spontaneous strain components of different leucite compounds. The total strain, ϵ_{tot} , may be rationalized as having two components: the volume-changing strain, ϵ_v , and the ferroelastic strain, ϵ_e . Rb- and Cs-substituted leucite show tricritical behavior, with $\epsilon \propto Q = (T - T_c)^{1/2}$. This is in marked contrast to KFeSi₂O₆ leucite, which shows slightly first-order behavior, where the temperature dependence of the order parameter (and hence the spontaneous strain) cannot be fitted to a simple power law. The results for natural leucite are plotted in Palmer et al. (1989). The graphs on the right side compare the behavior of the two strain components ϵ_v and ϵ_e .

is consistent with a diamond glide plane parallel to (110) . Finally, in the cubic, $Ia3d$, phase, the K ions are constrained to lie on-axis, parallel to the channel length.

Analogies between temperature and composition. At a structural level, we observe the same type of framework response to changing channel-cation size and changing temperature: a twisting of tetragonal prisms about $[001]$, illustrated in Figure 9. There must be an interaction between the changing framework distortion, which, because of the interconnected structure affects the channel size too, and the behavior of the K cations, which appear larger (and more mobile; Grögel et al. 1984; Palmer and Salje 1990) at high temperatures.

The T-O bond lengths are affected by both temperature and composition. Figure 10 shows the behavior of the mean T-O bond lengths as a function of temperature for natural leucite. (In the $I4_1/a$ leucite structure, there are three sets of tetrahedral sites, denoted T1, T2, and T3; at low temperatures, T1 is the smallest site.) All the T-O bond lengths decrease slightly with increasing tempera-

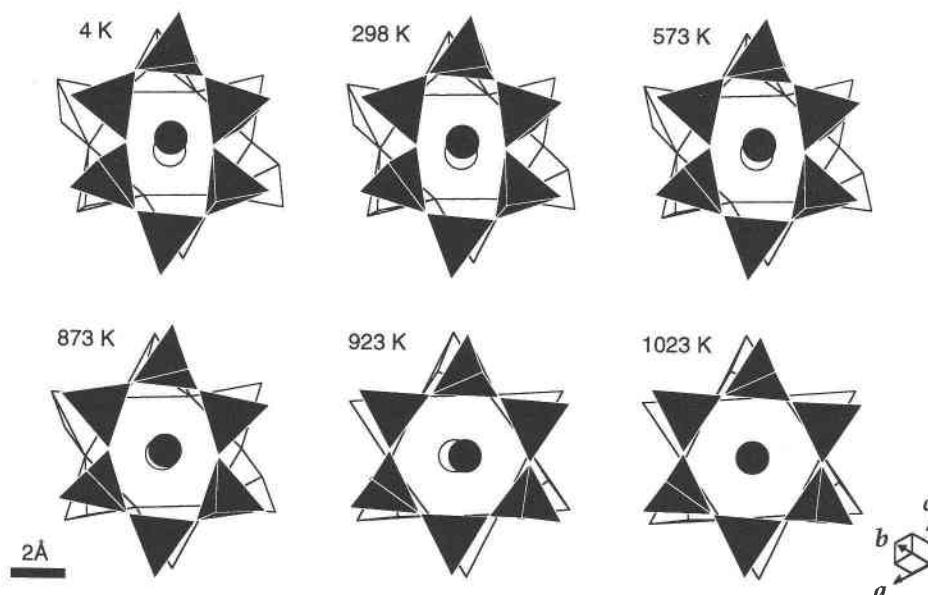


FIGURE 7. CrystalMaker (Palmer 1994) plots showing the leucite channel structure viewed parallel to $[1\bar{1}1]$ as a function of temperature. At low temperatures leucite has space group $I4_1/a$ with two kinds of sixfold tetrahedral rings, which act as “bottle-necks,” constricting the $\langle 111 \rangle$ structural channels. The upper ring is shown in black, the lower ring in white; the K^+ ions are plotted as circles and positioned above each of the sixfold rings. Crumpling of the sixfold rings forces the K^+ ions to move off

center, along the $[\bar{1}12]$ direction. At higher temperatures, the framework expands and the K^+ off-centering decreases. Note that the direction of the off-centering also changes. In the intermediate $I4_1/acd$ tetragonal phase (923 K), the $\langle 111 \rangle$ structural channels are fully inflated, and the off-centering of the K^+ channel cations is along $[110]$, perpendicular to the low-temperature distribution. In the high-temperature, $Ia3d$ cubic phase, the channel cations are, on average, arrayed centrally, along the channel axis.

ture. This decrease might be attributed to the “swinging bond” effect (Hazzen and Finger 1982) in which vibrations of O ions perpendicular to the mean T-O-T direction, lead to an apparent shortening of the T-O distance.

The use of substituted leucite allows us to provide an alternative explanation. The mean T-O distances (Table

6) decrease when the size of the channel cation increases. As the T-O distances decrease, the T-O-T angles increase as the channels inflate. This inverse correlation between T-O bond lengths and T-O-T bond angles is common in other framework silicates and is usually explained in terms of ionic repulsions forcing the cations further apart. Thus, increasing the T-O-T angles (as happens with increasing temperature and channel-cation size) might be expected to decrease the T-O bond lengths.

Although the correlation between T-O-T bond angles and T-O bond lengths is certainly a factor in determining the behavior of tetragonal leucite, it does not hold for the cubic phases. Here we find that T-O-T bond angles are virtually identical across the spread of compositions, yet T-O bond lengths vary widely.

The analogy between increasing cation size and increasing temperature is not sufficient to explain changes near the tetragonal-to-cubic phase transition. On increasing temperature, there is a very rapid change in unit-cell parameters near T_c (Fig. 5 and Palmer et al. 1989), which is not mirrored by the unit-cell and cation-size data (Fig. 4), which instead show a gradual convergence of a and c toward Cs-substituted leucite.

In addition to the A_{2g} rotational distortion of the $[001]$ prism elements already discussed, we believe that pure leucite shows an additional, ferroelastic (shear) distortion, with symmetry E_g , which leads to the rapid convergence of the unit-cell parameters a and c near T_c . The E_g dis-

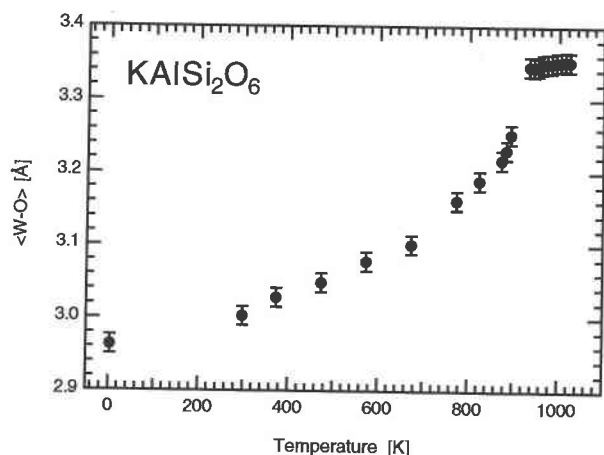


FIGURE 8. Mean K-O bond length plotted as a function of temperature for natural leucite. The mean bond length is the average of the six shortest distances to O atoms around the K channel cation. The trend reflects the continuing expansion of the $\langle 111 \rangle$ structural channels, with increasing temperature.

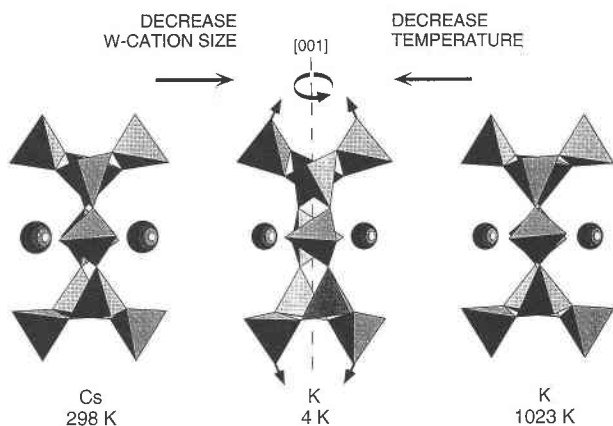


FIGURE 9. Distortion of the leucite structure induced by temperature or composition. The structure may be visualized in terms of tetragonal prisms with their long axes parallel to [001]. The view direction is [110]. The channel-cation sites, depicted as spheres, are connected by side channels passing through eightfold tetrahedral rings. Smaller channel cations (e.g., K replacing Cs), or reduced temperatures, induce a twisting distortion in the prisms (the upper ring rotates around [001], relative to the lower ring). This causes axial elongation, but radial compression. Metrically, c is extended, whereas a and b are decreased.

ortion may be visualized by considering the intermediate $I4_1/acd$ phase. Here, the structural channels are fully inflated (i.e., the A_{2g} distortion is zero). Any off-centering of K^+ in this phase must therefore directly reflect the nonzero E_g order parameter. This off-centering is orthogonal to that forced by channel collapse (i.e., the volume anomaly) at low temperatures, which must reflect the A_{2g} distortion pattern. We observed that on decreasing temperature, the actual direction of off-centering gradually rotates from the E_g position to that forced by a pure A_{2g} distortion (as displayed by Rb-substituted and Cs-substituted leucite samples). This changing offset pattern appears to represent a compromise between competing E_g and A_{2g} distortion patterns.

The increased framework distortion of $KFeSi_2O_6$ leucite, demonstrated by the small T-O-T bond angles (Table 7), provides an interesting analog for a hypothetical leucite structure with channel cations smaller than K^+ . In this sense, therefore, the series of leucite structures $KFeSi_2O_6$, $KAlSi_2O_6$, $RbAlSi_2O_6$, to $CsAlSi_2O_6$ is one of decreasing framework distortion and expanded channel network. It is interesting that the character of the phase transition changes throughout this series, from distinctly first order for $KFeSi_2O_6$, to tricritical for Rb- and Cs-substituted leucite. Natural leucite is an intermediate case, with its additional $I4_1/acd$ tetragonal phase, but still has an abrupt structural change near T_c .

LEUCITE CRYSTAL CHEMISTRY

Our aim is to explain the structural behavior of leucite in terms of its crystal-chemical aspects. In particular, two

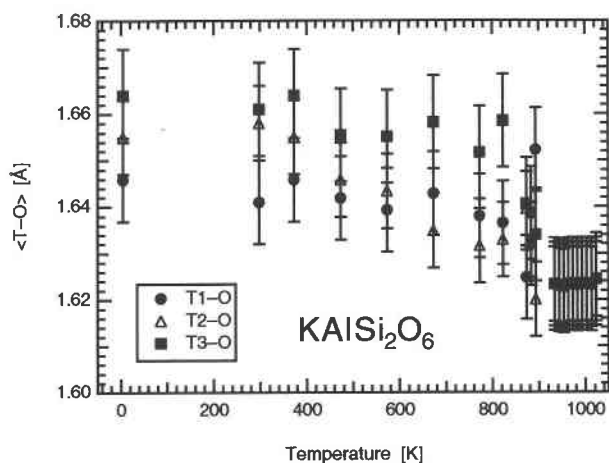


FIGURE 10. Temperature dependence of the mean T-O bond lengths for the three tetrahedral sites T1, T2, and T3. On increasing temperature, there is a decrease in the bond lengths, which becomes pronounced near the cubic-to-tetragonal phase-transition temperature.

questions must be addressed: (1) Can the phase transition be explained on crystal-chemical grounds? (2) Why should the cubic forms of different leucite compounds have different unit-cell volumes?

General trends

Figure 11a shows the relation between effective size of the channel cation (measured by the mean W-O bond length) and the mean unit-cell dimension (cube root of volume) for different leucite samples at different temperatures. There is a linear relation between $\langle W-O \rangle$ and the unit-cell dimension in the tetragonal phase; increasing the temperature causes both quantities to increase. The different tetragonal leucite phases lie on different lines in this diagram, but the data for all cubic leucite phases are colinear, so that increasing the temperature of cubic $KAlSi_2O_6$ leucite drives it toward Rb- and Cs-substituted leucite. Both leucite and $KFeSi_2O_6$ show discontinuities between the tetragonal and cubic phases; this is in contrast to Rb- and Cs-substituted leucite, for which tetragonal data extrapolate onto the cubic data.

Figure 11b shows the same data as Figure 11a, but tie-lines are drawn between data points for different leucite types. The exchange $Al^{3+} \rightarrow Fe^{3+}$ hardly changes $\langle W-O \rangle$ but greatly increases the unit-cell dimensions. It has already been shown that this is achieved by increasing the size of the tetrahedra (i.e., the $\langle T-O \rangle$ increase). By contrast, the exchange $K^+ \rightarrow Rb^+ \rightarrow Cs^+$ increases $\langle W-O \rangle$ and increases the unit-cell volume, with only a very small change in the $\langle T-O \rangle$ bond lengths. This has been shown to occur by tetrahedral tilting (twisting distortions of the tetragonal prism elements parallel to [001]), changing the size of the $\langle 111 \rangle$ channels.

The discontinuities observed between the tetragonal and cubic phases of $KAlSi_2O_6$ and $KFeSi_2O_6$ leucite may

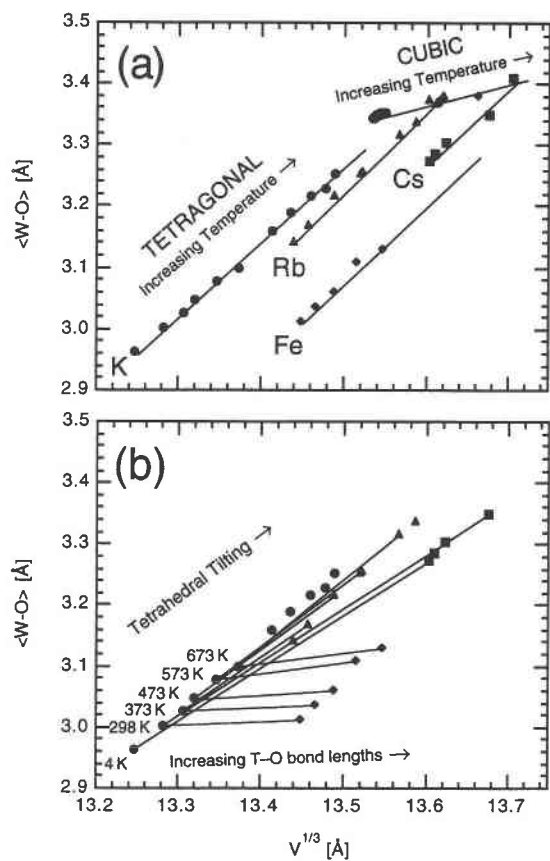


FIGURE 11. Effective size of the channel cation (measured by the mean W-O distance) plotted as a function of cell dimension (cube-root of volume) for different leucite compounds at different temperatures. (a) The effects of composition on the transition behavior. In comparison with Rb-substituted leucite (Rb), natural leucite (K) and KFeSi_2O_6 leucite (Fe) show large discontinuities between the low-temperature tetragonal phase and the high-temperature cubic phase (individual error bars are smaller than the symbols plotted). Note that the data for the cubic phases in each crystal are colinear. (b) Structural response of the tetragonal phase with respect to changing temperature and composition. Tie-lines are drawn between different leucite compounds at the same temperature. Changing the size of the channel cations causes tetrahedral tilting but virtually no change in T-O bond lengths. By contrast, substituting larger framework cations increases the T-O bond lengths but does not affect the tetrahedral tilting.

be attributed to first-order transition behavior or to an additional transition mechanism near T_c . For the KAlSi_2O_6 , it has already been shown that the E_g shear distortion becomes prominent near T_c . The E_g distortion alters the K distribution (and hence the W-O bond lengths) without significantly changing the unit-cell volume. We should also note that dielectric measurements (Palmer and Salje 1990) and anharmonic temperature-factor analysis (Boysen 1990) demonstrate partial delocalization of K at high temperatures, near T_c , which may serve to stabilize the intermediate phase of leucite.

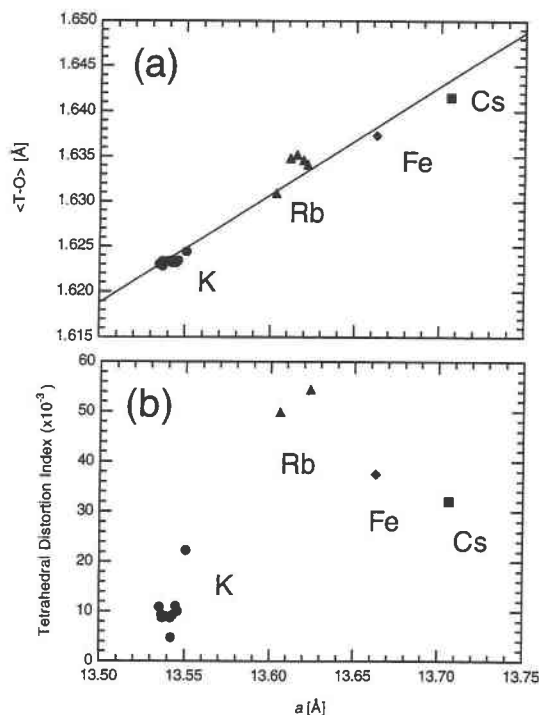


FIGURE 12. Parameters for the $(\text{Al,Si})\text{O}_4$ tetrahedra for the cubic phases of different leucite compounds as a function of unit-cell volume. (a) Mean T-O bond length. Increasing the temperature for natural leucite drives the structure toward those of Rb, Fe, and Cs analogs of leucite. (b) Tetrahedral distortion index, δ . There is little or no correlation between the distortion of the tetrahedra and the unit-cell volume. This confirms that thermal expansion in the cubic phase of leucite reflects the increasing size of the tetrahedral elements, not their changing shapes. Symbols are the same as for Figure 11.

Structural behavior of cubic leucite

The high-temperature, cubic phases of the leucite family appear identical, as required by symmetry, and the structural plots show that the $\langle 111 \rangle$ channels are fully expanded. However, there is a large increase in volume from $\text{K} \rightarrow \text{Rb} \rightarrow \text{Cs}$, or from $\text{KAl} \rightarrow \text{KFe}$ among cubic leucite. This (linear) trend is depicted in Figure 11a.

Because of the interconnected nature of the leucite framework, the only way in which the cubic unit-cell volume may be increased is by increasing the mean T-O bond lengths. The differences between KAlSi_2O_6 and KFeSi_2O_6 leucite are obvious: Fe^{3+} is larger than Al^{3+} and expands the tetrahedral framework. Less obvious, however, is the reason that the size of the channel cation should affect the volume of the cubic cell. It cannot be purely a cation-size effect because the framework is fully extended with no scope for polyhedral tilting. A possible explanation concerns rigid-unit mode vibrations (Dove et al. 1993b, 1995; Hammonds et al. 1996). On increasing temperature, there are two competing factors: thermal expansion of the T-O bond and increasing rotations of rigid tetrahedra. The latter would actually cause the cell size

to decrease; but increasing the size of the channel cations would hinder such vibrations, thereby effectively increasing the cell size (Fig. 12a).

Finally, we can investigate the distortion of the tetrahedra in the cubic phase by defining a tetrahedral distortion index, δ , which measures the difference in the T-O bond lengths for an individual tetrahedron:

$$\delta = \sqrt{\frac{4}{3} \sum_{i=1}^4 (t_i - \langle t \rangle)^2}$$

where t_i is the T-O_i bond length and $\langle t \rangle$ is the mean T-O bond length for that tetrahedron. For a perfect tetrahedron, $\delta = 0$. Figure 12b plots δ as a function of unit cell volume for different cubic leucite samples; the distortion index varies erratically with cell volume, so we may infer that any volume changes in the cubic phase do significantly modify tetrahedral distortions.

ACKNOWLEDGMENTS

We thank the U.K. Science and Engineering Research Council for HRPD beam time. M.T.D. is also grateful to SERC for travel costs to Chalk River, and to the staff of AECL Research for their hospitality. We thank Frances Wall (Natural History Museum, London) for her help with the analysis of the Cs- and Rb-substituted leucite, and Ciriaco Giampaolo (Universita di Roma) for his invaluable assistance with the collection of natural leucite from the Roman Volcanic District. During the experimental part of this work (1989–1990), D.C.P. was supported by a Bachelor Scholarship from Emmanuel College, Cambridge, and a Research Studentship from the Natural Environment Research Council.

REFERENCES CITED

- Bayer, G. (1973) Thermal expansion of new leucite-type compounds. *Naturwissenschaften*, 60, 102–103.
- Bell, A.M.T., and Henderson, C.M.B. (1994) Rietveld refinement of the structures of dry-synthesized $M\text{Fe}^{\text{III}}\text{Si}_2\text{O}_6$ leucites ($M = \text{K, Rb, Cs}$) by synchrotron X-ray powder diffraction. *Acta Crystallographica*, C50, 1531–1536.
- Boysen, H. (1990) Neutron scattering and phase transitions in leucite. In E.K.H. Salje, Ed., *Phase transitions in ferroelastic and coelastic crystals*, p. 334–349. Cambridge University Press, Cambridge.
- Brown, I.W.M., Cardile, C.M., MacKenzie, K.J.D., Ryan, M.J., and Meinhold, R.H. (1987) Natural and synthetic leucites studied by solid state ^{29}Si - and ^{27}Al NMR and ^{57}Fe Mossbauer spectroscopy. *Physics and Chemistry of Minerals*, 15, 78–83.
- Dove, M.T., Cool, T., Palmer, D.C., Putnis, A., Salje, E.K.H., and Winkler, B. (1993a) On the role of Al-Si ordering in the cubic-tetragonal phase transition of leucite. *American Mineralogist*, 78, 486–492.
- Dove, M.T., Giddy, A.P., and Heine, V. (1993b) Rigid unit mode model of displacive phase transitions in framework silicates. *Transactions of the American Crystallographic Association*, 27, 65–75.
- Dove, M.T., Heine, V., and Hammonds, K.D. (1995) Rigid unit modes in framework silicates. *Mineralogical Magazine*, 59, 629–639.
- Faust, G.T. (1936) The fusion relations of iron-orthoclase. *American Mineralogist*, 21, 735–763.
- (1963) Phase transition in synthetic and natural leucite. *Schweizerische Mineralogische und Petrographische Mitteilungen*, 43, 165–195.
- Galli, E., Gottardi, G., and Mazzi, F. (1978) The natural and synthetic phases with the leucite framework. *Mineralogica et Petrographica Acta*, 22, 185–193.
- Grögel, T., Boysen, H., and Frey, F. (1984) Neutron powder investigation of $I4_1/a-Ja3d$ in leucite. The 13th International Congress of Crystallography, C256–257.
- Hamilton, D.L., and Henderson, C.M.B. (1968) The preparation of silicate compositions by a gelling method. *Mineralogical Magazine*, 36, 832–838.
- Hammonds, K., Dove, M., Giddy, A., Heine, V., and Winkler, B. (1996) Rigid-unit phonon modes and structural phase transitions in framework silicates. *American Mineralogist*, 81, 1057–1079.
- Hatch, D.M., Ghose, S., and Stokes, H.T. (1990) Phase transitions in leucite, KAlSi_3O_8 : I. Symmetry analysis with order parameter treatment and the resulting microscopic distortions. *Physics and Chemistry of Minerals*, 17, 220–227.
- Hazen, R.M., and Finger, L.W. (1982) *Comparative crystal chemistry*, 231 p. Wiley, New York.
- Heaney, P.J., and Veblen, D.R. (1990) A high-temperature study of the low-high leucite phase transition using the transmission electron microscope. *American Mineralogist*, 75, 464–476.
- Hirao, K., Soga, N., and Kunugi, M. (1976) Thermal expansion and structure of leucite-type compounds. *Journal of Physical Chemistry*, 80, 1612–1616.
- Hirao, K., and Soga, N. (1982) The heat capacity and a phase transition in leucite-type compounds. *Yogyo-Kyokai-Shi*, 90(7), 390–396.
- Kosorukov, A.A., and Nadal, L.G. (1986) High-temperature X-ray diffraction of synthetic leucite, $\text{Rb}[\text{AlSi}_3\text{O}_8]$ and pollucite. *Soviet Physics—Crystallography*, 31(2), 148–151.
- Lange, R.A., Carmichael, I.S.E., and Stebbins, J.F. (1986) Phase transitions in leucite KAlSi_3O_8 , orthorhombic KAlSiO_4 , and their iron analogues (KFeSi_3O_8 , KFeSiO_4). *American Mineralogist*, 71, 937–945.
- Mazzi, F., Galli, E., and Gottardi, G. (1976) The crystal structure of tetragonal leucite. *American Mineralogist*, 61, 108–115.
- Merlino, S. (1984) Feldspatoids: Their average and real structures. In W.L. Brown, Ed., *Feldspars and feldspatoids*, p. 435–470. Reidel, Dordrecht, The Netherlands.
- Murdoch, J.B., Stebbins, J.F., Carmichael, I.S.E., and Pines, A. (1988) A silicon-29 nuclear magnetic resonance study of silicon-aluminum ordering in leucite and analcite. *Physics and Chemistry of Minerals*, 15, 370–382.
- Palmer, D. (1990a) Volume anomaly and the impure ferroelastic phase transition in leucite. In E.K.H. Salje, Ed., *Phase transitions in ferroelastic and coelastic crystals*, p. 350–366. Cambridge University Press, Cambridge.
- (1990b) Phase transitions in leucite. Ph.D. thesis, University of Cambridge, Cambridge, U.K.
- (1994) *CrystalMaker: Interactive crystallography for Macintosh and Power Macintosh*. Lynxvale Ltd., Cambridge, U.K.
- Palmer, D.C., Putnis, A., and Salje, E.K.H. (1988) Twinning in tetragonal leucite. *Physics and Chemistry of Minerals*, 16, 298–303.
- Palmer, D.C., Bismayer, U., and Salje, E.K.H. (1990) Phase transitions in leucite: Order parameter behavior and the Landau potential deduced from Raman spectroscopy and birefringence studies. *Physics and Chemistry of Minerals*, 17, 259–265.
- Palmer, D.C., and Salje, E.K.H. (1990) Phase transitions in leucite: Dielectric properties and transition mechanism. *Physics and Chemistry of Minerals*, 17, 444–452.
- Palmer, D.C., Salje, E.K.H., and Schmah, W.W. (1989) Phase transitions in leucite: X-ray diffraction studies. *Physics and Chemistry of Minerals*, 16, 714–719.
- Peacor, D.R. (1968) A high temperature single crystal diffractometer study of leucite, $(\text{K,Na})\text{AlSi}_3\text{O}_8$. *Zeitschrift für Kristallographie*, 127, 213–224.
- Phillips, B.L., Kirkpatrick, R.J., and Putnis, A. (1989) Si,Al ordering in leucite by high-resolution ^{27}Al MAS NMR spectroscopy. *Physics and Chemistry of Minerals*, 16, 591–598.
- Phillips, B.L., and Kirkpatrick, R.J. (1994) Short-range Si-Al order in leucite and analcime: Determination of the configurational entropy from ^{27}Al and variable-temperature ^{29}Si NMR spectroscopy of leucite, its Cs- and Rb-exchanged derivatives, and analcime. *American Mineralogist*, 79, 1025–1031.
- Shannon, R.D. (1976) Revised effective ionic radii and systematic studies of interatomic distances in halides and chalcogenides. *Acta Crystallographica*, A23, 751–761.
- Taylor, D., and Henderson, C.M.B. (1968) The thermal expansion of the leucite group of minerals. *American Mineralogist*, 53, 1476–1489.